DOI 10.1007/s11237-022-09746-1
Theoretical and Experimental Chemistry, Vol. 58, No. 4, September, 2022 (Ukrainian Original Vol. 58, No. 4, July-August, 2022)

INFLUENCE OF ACID–BASE PROPERTIES OF MFe_2O_4 FERRITES (M(II) = Fe, Mg, Mn, Zn) ON THEIR SELECTIVITY IN THE CONVERSION OF ETHANOL TO ACETONE

L. Yu. Dolgikh, I. L. Stolyarchuk, L. O. Stara, L. M. Senchylo, and Y. I. Pyatnitsky

UDC 544.47:544.344

The acidity and basicity of MFe_2O_4 (M(II) = Fe, Mg, Mn, Zn) ferrites of the spinel structure have been characterized by temperature-programmed desorption of NH_3 and CO_2. It is shown that both medium-strength basic and acid sites play an important role in the process of acetone obtaining from ethanol over ferrites. The selectivity of ethanol conversion to acetone depends both on the acid–base properties of the surface and on the ability of the surface oxygen of ferrite to participate in the intermediate redox stages of formation and steam reforming of acetone.

Keywords*: ethanol, acetone, catalyst, ferrites, temperature-programmed desorption, acid–base properties.*

Acetone is a valuable solvent and substance for organic synthesis [1-3], as well as an intermediate compound for ethanol conversion to an industrially important product, such as propene [4-6]. Propene demand is constantly growing [7], which promotes the development of alternative methods of its production. The catalytic process of ethanol-to-propene conversion (ETP) is one of the methods that use bioethanol as a renewable raw material. The reaction pathway of the ETP process over metal oxide catalysts includes ethanol dehydrogenation to acetaldehyde, acetaldehyde conversion to acetone, acetone hydrogenation to isopropanol, and isopropanol dehydration to propene [8]. Therefore, a two-stage catalytic ETP process was proposed to increase propene selectivity, the first stage of which includes ethanol conversion to acetone [9, 10].

Metal ferrites that can be used to produce significant amounts of acetone may serve as potential catalysts for the first stage [11]. It is known that the activity and selectivity of ethanol conversion catalysts depend on the acid–base characteristics of their surface [12-15]. This work aims at determining the dependence of selectivity of catalytic conversion of ethanol to acetone over MFe_2O_4 spinel structure ferrites (M(II) = Fe, Mg, Mn, and Zn) on their acid–base properties.

EXPERIMENTAL

The preparation method of used ferrites and the control of their phase composition is described in [16].

The acid–base properties of the surface of the catalysts were determined by temperature-programmed desorption of ammonia (TPD-NH_3 and CO_2 (TPD-CO_2) using a thermal conductivity detector (TCD). A catalyst sample was treated in He flow (40 mL/min) at 823 K for 2 h, then cooled to 323 K. Adsorption of NH_3 or CO_2 was performed at 323 K from a mixture of

L. V. Pisarzhevskii Institute of Physical Chemistry, NAS of Ukraine, Kyiv, Ukraine. E-mail: Dolgih.L.Ju@nas.gov.ua.
Translated from Teoretychna ta Eksperymentalna Khimiya, Vol. 58, No. 4, pp. 259-264, July-August, 2022. Received July 25, 2022; accepted September 9, 2022.

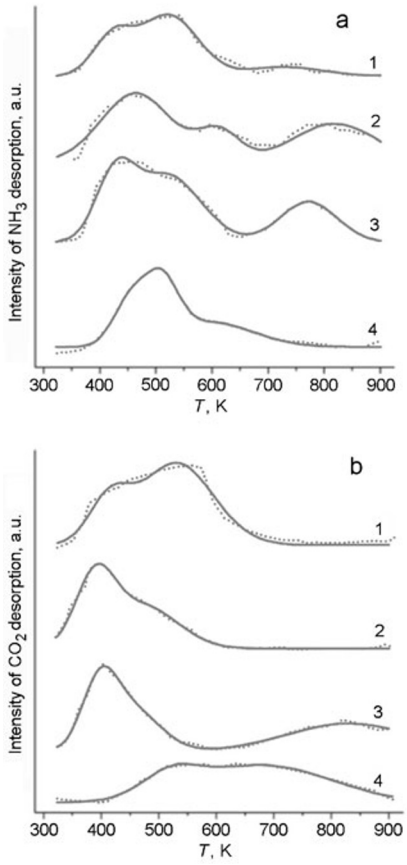

Fig. 1. TPD-NH_3 (a) and TPD-CO_2 (b) profiles from the surface of spinels: 1) $FeFe_2O_4$; 2) $MgFe_2O_4$; 3) $MnFe_2O_4$; 4) $ZnFe_2O_4$ (dotted line is an experimental curve, solid line is a calculated curve).

10vol.%NH_3/He or of 10vol.%CO_2/He for 30 min followed by He blowing for 2 h. NH_3 (CO_2) desorption was performed in the range of 323-923 K at a temperature rise rate of 10 K/min in He flow (40 mL/min).

Desorption profiles were decomposed by Gaussian functions to determine weak, medium, and strong acid and basic sites. The total amount of desorbed NH_3 and CO_2 was calculated by integrating the corresponding temperature-programmed desorption profiles using calibration coefficients, which were determined by passing known amounts of NH_3 or CO_2 through the TCD.

The catalytic process of ethanol conversion was performed in a flow quartz reactor under atmospheric pressure. The methodology of catalytic tests and analysis of the reaction mixture is described in [16].

RESULTS AND DISCUSSION

TPD-NH_3 profiles from the surface of MFe_2O_4 samples (M(II) = Fe, Mn, Mg, and Zn) are presented in Fig. 1a. They have a complex shape, which indicates the presence of several types of acid sites on the surface of the studied ferrospinels. It is known that NH_3 reacts with the surface of oxides with the participation of hydrogen OH groups (Bronsted acid sites) and coordinatively unsaturated metal cations (Lewis acid sites) [17]. Therefore, TPD-NH_3 profiles were decomposed, assuming the presence of three types of acid sites in ferrites, namely surface metal M^{2+}, M^{3+} cations and OH groups.

TABLE 1. Acid–Base Characteristics of Ferrites According to TPD-NH_3 and TPD-CO_2 Data

Ferrite	Relative amount of desorbed NH_3, %			Total amount of desorbed NH_3, $mmol \cdot g^{-1}$	Relative amount of desorbed CO_2, %			Total amount of desorbed CO_2, $mmol \cdot g^{-1}$	Ratio of desorbed CO_2 and NH_3
	$T(NH_3)_l$ 423—503 K	$T(NH_3)_m$ 523—673 K	$T(NH_3)_h$ 723—823 K		$T(CO_2)_l$ 373—423 K	$T(CO_2)_m$ 443—673 K	$T(CO_2)_h$ 723—823 K		
$FeFe_2O_4$	25.8	62.1	12.1	0.98	21.3	78.7	–	0.22	0.23
$MgFe_2O_4$	53.8	14.7	31.5	1.31	46.2	53.8	–	1.16	0.12
$MnFe_2O_4$	25.1	49.9	25.0	1.57	29.6	33.9	36.5	0.20	0.13
$ZnFe_2O_4$	70.3	29.7	–	0.97	–	74.8	25.2	0.09	0.09

The presence of two maxima at temperatures of 423 and 522 K, as well as a weak high-temperature peak at 729 K was established by the Gaussian-function-based deconvolution method in the TPD-NH_3 profile of complex iron oxide $FeFe_2O_4$ (Fig. 1a, curve 1). Maxima at 464 and 612 K and a high-temperature peak at 819 K were detected for $MgFe_2O_4$ (Fig. 1a, curve 2). The $MnFe_2O_4$ profile (Fig. 1a, curve 3) has three peaks with maximum temperatures of 427, 520, and 772 K. Peaks at 491 and 622 K are observed for $ZnFe_2O_4$ (Fig. 1a, curve 4).

There are three temperature regions of NH_3 desorption from the surface of the studied ferrospinels. Table 1 shows the desorption intervals from low ($T(NH_3)_l$), medium ($T(NH_3)_m$), and high-temperature ($T(NH_3)_h$) sites and the relative amounts of such sites.

The first (low-temperature) region covers the interval of 423-503 K and is associated with NH_3 desorption from weak acid OH groups and partially the release of physically adsorbed ammonia. The relative number of such sites prevails in the acidity spectra of $MgFe_2O_4$ and $ZnFe_2O_4$. The second (medium-temperature) region covers the range of 523-673 K. The desorption peaks observed at these temperatures characterize medium-strength acid sites, probably coordinatively unsaturated Fe^{2+}, Mg^{2+}, Mn^{2+}, and Zn^{2+} cations. The relative number of such sites is the largest for $FeFe_2O_4$ and $MnFe_2O_4$. The desorption peaks in the third (high-temperature) region at 723-823 K of the TPD-NH_3 profiles of Fe, Mg, and Mn ferrites characterize NH_3 desorption from strong acid sites associated with Fe^{3+} cations.

TPD-CO_2 profiles from the surface of MFe_2O_4 samples (M(II) = Fe, Mn, Mg, and Zn) are shown in Fig. 1b. The complex shape of the profiles indicates CO_2 desorption from different strength basic sites of the surface of ferrospinels. It is known that CO_2 reacts with the surface of oxides in different ways, in particular with the participation of surface hydroxyl groups, surface oxygen or metal–oxygen pairs with the formation of bicarbonates, or mono- and bidentate surface compounds [13, 17]. Therefore, an analysis of the TPD-CO_2 profiles was performed for three types of basic sites.

The broad peak of CO_2 desorption from the $FeFe_2O_4$ surface is decomposed into peaks with maxima at 413 and 530 K (Fig. 1b, curve 1). Peaks with maxima at 390 and 472 K, 397 and 452 K were detected for $MgFe_2O_4$ and $MnFe_2O_4$, respectively (Fig. 1b, curves 2 and 3). In addition, the TPD-CO_2 profile for $MnFe_2O_4$ contains a peak with a maximum at 830 K. There are no low-temperature peaks in the desorption profile for $ZnFe_2O_4$, however, a broad peak, that can be decomposed into several components with maxima at 515, 640, and 788 K, is recorded (Fig. 1b, curve 4).

The obtained results allow to distinguish three temperature regions of CO_2 desorption from the surface of ferrospinels. The intervals of CO_2 desorption from the low ($T(CO_2)_l$), medium ($T(CO_2)_m$), and high-temperature ($T(CO_2)_h$) sites and the relative numbers of *l, m*, and *h* sites are shown in Table 1.

The low-temperature region covers the range of 373-423 K and characterizes the decomposition of surface bicarbonates, which are formed due to CO_2 adsorption on weak basic OH groups of the surface [11, 18, 19]. These CO_2 desorption peaks are observed in the $FeFe_2O_4$, $MnFe_2O_4$, and $MgFe_2O_4$ profiles. Peaks in the medium-temperature region of 443-673 K can be attributed to the decomposition of bidentate carbonate particles, which are formed during the interaction of

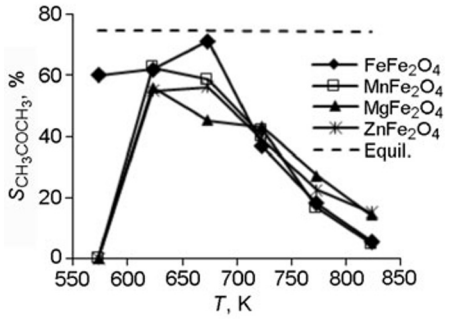

Fig. 2. Temperature dependence of acetone selectivity over $FeFe_2O_4$, $MnFe_2O_4$, $MgFe_2O_4$, and $ZnFe_2O_4$ ferrites; initial reaction mixture: 2.7 mole % of C_2H_5OH, 50 mole % of H_2O, and N_2 as the remainder; atmospheric pressure (dashed line indicates the equilibrium selectivity value for acetone, calculated for reactions (I) and (II) according to the method [10]).

CO_2 with metal–oxygen pairs on the surface of ferrites. These desorption peaks are typical for all the samples and form the main part of the basicity spectrum of $FeFe_2O_4$, $MgFe_2O_4$, and $ZnFe_2O_4$ ferrites. The high-temperature region (T > 723 K) characterizes monodentate forms of CO_2 adsorption with the participation of ferrite surface oxygen. Such forms are typical for $MnFe_2O_4$ and $ZnFe_2O_4$ samples. At the same time, the fact that the desorption peaks at temperatures of 800 K for the mentioned ferrites may be partially related to the decomposition of bulk iron carbonates cannot be excluded.

The acid–base properties of ferrites can significantly affect the conversion of ethanol on their surface. The first stage of the two-stage process of ethanol conversion to propene [9, 10] consists of the following main reactions:

$$C_2H_5OH = CH_3CHO + H_2, \quad \text{(I)}$$

$$2CH_3CHO + H_2O = CH_3COCH_3 + CO_2 + 2H_2. \quad \text{(II)}$$

Figure 2 shows the dependence of acetone selectivity ($S_{CH_3COCH_3}$) on the temperature in the process of ethanol conversion on the studied ferrites (selectivity is defined as the mole fraction of ethanol converted to acetone).

The temperature dependence of acetone selectivity is characterized by a maximum; the decrease of $S_{CH_3COCH_3}$ at elevated temperatures is associated with an increasing rate of further acetone conversion. The highest acetone selectivity is achieved over iron ferrite $FeFe_2O_4$ at 673 K that is quite close to the selectivity equilibrium value, in particular, the subsequent conversion of acetone is still slowed down at this temperature.

The literature provides several reaction pathways for ethanol conversion to acetone over oxides and metal catalysts deposited on oxide carriers. The first stage, ethanol dehydrogenation to acetaldehyde, is common for all proposed reaction schemes.

One of the paths of further conversion of acetaldehyde to acetone is the reaction of direct coupling of two acetaldehyde molecules (aldol condensation) with the formation of 3-hydroxybutylaldehyde (acetaldol), its dehydrogenation and decarboxylation [6, 20-22]:

$$2CH_3CHO \leftrightarrow CH_3CH(OH)CH_2CHO,$$

$$CH_3CH(OH)CH_2CHO \leftrightarrow CH_3COCH_2CHO + H_2,$$

$$CH_3COCH_2CHO + H_2O = CH_3COCH_3 + CO_2 + H_2.$$

Another path is the oxidation reaction of acetaldehyde to acetic acid followed by its ketonization [8, 23, 24]:

$$CH_3CHO + H_2O \leftrightarrow CH_3COOH + H_2,$$

$$2CH_3COOH \leftrightarrow CH_3COCH_3 + CO_2 + H_2O.$$

Some authors assume that the initial stage includes the dimerization of acetaldehyde with the formation of ethyl acetate (Tishchenko reaction), its conversion to acetic acid, and ketonization [8, 25-27]:

$$2CH_3CHO \leftrightarrow CH_3COOC_2H_5 \text{ (Tishchenko reaction)},$$

$$CH_3COOC_2H_5 \leftrightarrow CH_3COOH + C_2H_4,$$

$$2CH_3COOH \leftrightarrow CH_3COCH_3 + CO_2 + H_2O.$$

The formation of acetone by the reaction between ethanol with acetaldehyde is proposed in work [28]:

$$C_2H_5OH + CH_3CHO \rightarrow CH_3COCH_3 + CO_2 + H_2O.$$

Aldol condensation of acetaldehyde with subsequent oxidation of acetaldol and decomposition with the formation of acetone, CO_2, and H_2 is the most probable reaction pathway for acetone synthesis from ethanol over ferrite catalysts considering that acetic acid and ethyl acetate were not observed in the products of ethanol conversion over ferrites, as well as a high content of water vapor in the reaction mixture under the studied conditions.

At the first stage of this process, ethanol is dissociatively adsorbed on the oxide surface with the formation of an intermediate ethoxy particle $CH_3CH_2O_{(a)}$ located on a metal ion and a proton located on a surface oxygen ion. Then, α-elimination of hydrogen from the C–H bond in the ethoxy particle occurs with the participation of another oxygen ion and the formation of adsorbed acetaldehyde. Hydrogen is desorbed from the surface in the form of H_2 or H_2O molecules [13, 32].

Adsorbed acetaldehyde can desorb into the gas phase or undergo conversion to more oxidized forms, such as adsorbed acetyl particles $C_2H_3O_{(a)}$ by detaching an additional hydrogen atom and acetate particles $CH_3COO_{(a)}$ by oxidation with the participation of hydroxyl groups or oxygen of the catalyst surface [29].

$CH_3CH_2O_{(a)}$ particles also lead to further reaction paths, in particular to the formation of acetone through an aldol-type mechanism [22]:

$$2CH_3–CHO_{(a)} + O_{(s)} \leftrightarrow CH_3–CH(OH)–CH_2–COO_{(a)} + H_{(a)},$$

$$CH_3–CH(OH)–CH_2–COO_{(a)} + H_{(a)} \leftrightarrow CH_3–CO–CH_3 + CO_2 + H_2 + \square_{(s)},$$

where $O_{(s)}$ is a surface oxygen atom, $\square_{(s)}$ is a surface oxygen vacancy.

The total reaction is

$$2CH_3–CHO_{(a)} + O_{(s)} \leftrightarrow CH_3–CO–CH_3 + CO_2 + H_2 + \square_{(s)}.$$

The loss of oxygen is compensated by the interaction of water with surface oxygen vacancies:

$$H_2O + \square_{(s)} \leftrightarrow O_{(s)} + H_2,$$

resulting in reaction (II).

According to the literature data, heterogeneous catalytic dehydrogenation of alcohols to aldehydes and coupling reactions require a specific configuration of pairs of acid–base sites consisting of Lewis acid sites and Bronsted basic sites [12, 30, 31]

The presence of such acid–base pairs of a certain strength on the surface of studied ferrites is confirmed by the results of TPD-CO_2 and TPD-NH_3. Surface metal cations $M^{\sigma+}$ in ferrites can be attributed to Lewis acid sites, while oxygen anions $O^{\sigma-}$ can be attributed to Bronsted basic sites. According to the obtained data, the majority of acid–base sites on the surface of the studied ferrites consist of medium-strength basic sites and strong basic sites, as well as weak and medium-strength acid sites. According to the literature data [13, 30, 32], such the sites play a key role in ethanol conversion over oxide catalysts. The ratio of the number of basic and acid sites, which is characterized by the ratio of the amounts of desorbed CO_2 and NH_3 (Table 1), has the largest value for $FeFe_2O_4$ and decreases in the following order: $FeFe_2O_4 > MnFe_2O_4 \sim MgFe_2O_4 > ZnFe_2O_4$.

A comparison of the acid–base and catalytic properties of ferrites showed that the $FeFe_2O_4$ catalyst, which is characterized by the highest acetone selectivity (71.3%), has the largest relative number of medium-strength basic and acid sites. A 63% acetone selectivity was achieved over $MnFe_2O_4$ ferrite. A significant number of medium-strength acid sites are present on its surface, however, the basicity spectrum, unlike $FeFe_2O_4$, is mainly represented by both medium-strength sites and strong basic sites. Lower acetone selectivity values that do not exceed 56% are observed for $MgFe_2O_4$ and $ZnFe_2O_4$ samples, which have mainly medium-strength basic sites on the surface and a low relative number of medium-strength acid sites. Therefore, both medium-strength basic and acid sites are important for the obtaining of acetone from ethanol over spinel structure ferrites. Ferrites that are characterized by a higher ratio of basic and acid sites, as well as a larger amount of the medium-strength acid sites show a higher selectivity for the target product in the process of ethanol conversion to acetone. It should be noted that the bimolecular reaction of aldol condensation requires not only acid–base sites of the catalyst surface but also the appropriate arrangement of atoms for the adsorption of reagents and intermediate compounds on nearby active sites [30].

The process of ethanol or acetaldehyde conversion to acetone also includes conversion with the participation of the surface oxygen of a catalyst, in particular in the stages of oxidation of adsorbed acetaldehyde or acetaldol [1, 2, 22, 32]. The process of steam reforming of acetone to CO_2 and H_2 over ferrites becomes significant under conditions of elevated temperatures (>673 K) [16]:

$$CH_3COCH_3 + 5H_2O = 3CO_2 + 8H_2.$$

Therefore, the rate of the surface reactions that compile the process of acetone obtaining from ethanol and the steam reforming of acetone depend significantly on the redox properties of a catalyst, namely on its ability to easily give up oxygen for the oxidation of surface reaction intermediates (reducibility of a catalyst). The results of the research of the ferrites by temperature-programmed reduction showed [11] that the nature of metal in the composition of ferrospinels significantly affects the reducibility of Fe^{3+} cations of the spinel crystal lattice. There is a decrease in the maximum temperature of Fe(III) → Fe(II) reduction when Mn, Mg, and Zn are added to the composition of a ferrospinel that characterizes the strength of the oxygen bond of a catalyst. The lowest value of the reduction maximum temperature was established for $MnFe_2O_4$ that indicates the higher oxygen reactivity of this catalyst when compared to Zn- and Mg-ferrospinels containing cations of constant valence. The study of catalytic properties showed that $FeFe_2O_4$ and $MnFe_2O_4$ are highly active in the process of acetone formation, which are characterized by the presence of both Fe^{3+} and Mn^{2+} and Fe^{2+} ions in the octahedral sublattice, which accelerates redox transformations of M^{3+}/M^{2+} and stages involving surface oxygen of a catalyst. At the same time, the processes of oxidation of intermediate compounds on the surface of $MnFe_2O_4$, $MgFe_2O_4$, and $ZnFe_2O_4$ are performed at a higher rate than the desorption of acetone into the gas phase, that reduces the selectivity for the target product.

The process of catalytic conversion of ethanol to acetone over ferrites includes several elementary reactions that involve the formation of various intermediate compounds with the participation of acid–base and redox sites of a catalyst. High (close to equilibrium) acetone selectivity is achieved over $FeFe_2O_4$; ferrites containing other metals (Mn, Mg, and Zn) show lower selectivity. In general, the obtained results indicate that the selectivity of ethanol conversion to acetone over ferrites is determined by the combined effect of the following factors: the presence of medium-strength basic and acid sites on the surface of a catalyst; the ability of surface oxygen of a catalyst to participate in redox processes.

REFERENCES

1. A. F. F. De Lima, C. R. Moreira, O. C. Alves, et al., *Appl. Catal. A.*, **611**, 117949 (2021).
2. C. P. Rodrigues, P. C. Zonetti, and L. G. Appel, *Chem. Cent. J.,* **11**, 30 (2017).
3. L. R. Silva-Calpa, P. C. Zonetti, D. C. Oliveira, et al., *Catal. Today*, **289**, 264-272 (2017).
4. X. Li, A. Kant, Y. He, et al., *Catal. Today,* **276**, 62-77 (2016).
5. V. Zacharopoulou and A. A. Lemonidou, *Catalysts*, **8**, 2-19 (2018).
6. R. Huang, V. Fung, Z. Wu, and D. Jiang, *Catal. Today*, **350**, 19-24 (2019).
7. F. Hayashi, M. Tanaka, D. Lin, and M. Iwamoto, *J. Catal.*, **316**, 112-120 (2014).
8. M. Iwamoto, *Catal. Today*, **242**, 243-248 (2015).
9. Y. Pyatnitsky, L. Dolgikh, L. Senchylo, et al., *Theor. Exp. Chem*., **55**, 50-55 (2019).
10. Y. Pyatnitsky, L. Dolgikh, L. Senchylo, et al., *Chem. Pap.,* **75**, 5773-5779 (2021).
11. L. Y. Dolgikh, I. L. Stolyarchuk, L. A. Staraya, et al., *Theor. Exp. Chem*., **54**, 349-357 (2018).
12. T. Nakajima, H. Nameta, S. Mishima, et al., *J. Mater. Chem*., **4**, 853-858 (1994).
13. J. I. Di Cosimo, V. K. Diez, M. Xu, et al., *J. Catal*., **178**, 499-510 (1998).
14. H. Song, L. Zhang, and U. S. Ozkan, *Top. Catal*., **55**, 1324-1331 (2012).
15. J. Sun, K. Zhu, F. Gao, et al., *J. Am. Chem. Soc*., **133**, 11096-11099 (2011).
16. I. L. Stolyarchuk, L. Yu. Dolgykh, I. V. Vasylenko, et al., *Theor. Exp. Chem*., **52**, 246-251 (2016).
17. A. Auroux and A. Gervasini, *Phys.Chem.*, **94**, 6371-6379 (1990).
18. M. B. Jensen, L. G. M. Pettersson, O. Swang, et al., *J. Phys. Chem. B.*, **109**, 16774-16781 (2005).
19. V. K. Diez, C. R. Apestegua, and J. I. Di Cosmo, *J. Catal.*, **240**, 235-244 (2006).
20. R. S. Murthy, P. Patnaik, P. Sidheswaran, et al., *J. Catal.*, **109**, 298-302 (1988).
21. K. Inui, T. Kurabayashi, and S. Sato, *J. Catal*., **212**, 207-215 (2002).
22. T. Nishiguchi, T. Matsumoto, H. Kanai, et al., *Appl. Catal. A*., **279**, 73-77 (2005).
23. T. Nakajima, K. Tanabe, T. Yamaguchi, et al., *Appl. Catal.*, **52**, 237-248 (1989).
24. J. Bussi, S. Parodi, B. Irigaray, et al., *Appl. Catal. A.*, **172**, 117-129 (1998).
25. H. Hattori, *Chem. Rev.*, **95**, 537-558 (1995).
26. F. Hayashi, M. Tanaka, D. Lin, et al., *J. Catal.*, **316**, 112-120 (2014).
27. G. G. Gonzalez, P. C. Zonetti, E. B. Silveira, et al., *J. Catal.*, **380**, 343-351 (2019).
28. K. Takeshita, S. Nakamura, and K. Kawamoto, *Bull. Chem. Soc. Jpn.*, **51**, 2622-2627 (1978).
29. L. V. Mattos, G. Jacobs, B. H. Davis, et al., *Chem. Rev.,* **112**, 4094-4123 (2012).
30. J. I. Di Cosmo, C. R. Apesteguia, M. J. L. Gines, et al., *J. Catal.*, **190**, 261-275 (2000).
31. M. V. Ganduglia-Pirovano, *Catal. Today,* **253**, 20-32 (2015).
32. J. E. Rorrer, F. D. Toste, and A. T. Bell, *ACS Catal.*, **9**, 10588-10604 (2019).